

# A Compact UWB DRA MIMO Antenna Realizing Band Notch Characteristics and Fractal Inspired Isolation Mechanism

Anindita Bhattacharjee<sup>1</sup>, Anirban Karmakar<sup>1, \*</sup>, and Anuradha Saha<sup>2</sup>

**Abstract**—In this communication, a new compact UWB dual port multiple-input multiple-output (MIMO) antenna is presented for wireless application. The design utilizes the property of dielectric resonator to achieve a bandwidth that ranges from 3.1 GHz to 18.5 GHz. The design has a compact size of  $19 \times 30 \times 0.8 \text{ mm}^3$ . It consists of two rectangular shape monopole antenna elements with rectangular dielectric resonators sharing a similar ground plane. On the ground plane, a modified Hilbert curve with a meander line parasitic element was introduced to improve isolation between radiating elements which reduces mutual coupling issues. A band notch is achieved at WLAN band (5.09–5.8 GHz) by etching a pair of L-shape slots on each radiator. The gain of the antenna drops significantly at the centre of the notch band which indicates good interference suppression. Results show that the designed antenna provides a wide impedance bandwidth (below  $-10 \text{ dB}$ ) throughout the operating band of 3.1–18.5 GHz (142.6%). The antenna also produces nearly  $-20 \text{ dB}$  isolation for the entire operating band. Results show that the simulated characteristics are in good agreement with the measured counterpart.

## 1. INTRODUCTION

Nowadays in wireless communication systems, it is essential to have a system with some attractive properties like high data rate, high channel capacity, and high reliability within the required power limit. Ultra-wideband (UWB) is a promising technology for personal area networks because of its appealing properties including high data rate and minimal operational power. Following the (Federal Communication Commission) FCC's publication of UWB regulations in 2002 [1], there has been a significant rise in research on the design of low-cost UWB antennas. Recently, it has been discovered that single antenna elements can suffer from multipath fading effect. As a result, MIMO/diversity UWB antenna design becomes necessary which connects multiple radiators at the transmitter as well as at the receiver side [2]. Due to this, the system channel capacity is also enhanced without requiring additional power [3]. The design issue entails creating multiple-input-multiple-output (MIMO) antennas with low correlation coefficients and low mutual coupling. Additionally, wideband MIMO antennas are required to achieve a high data rate without increasing the power level [4].

In recent years, various researchers have proposed several MIMO antennas for wideband application. Owing to the speedy expansion of communication systems, the researchers focused on wideband as well compact antenna design. In [5], a two-port MIMO antenna is presented for wideband application. The designed antenna comprises two identical shape monopoles to improve the isolation performance where two novel slits and triangles are cut from the ground plane. In [6], a MIMO antenna with fence-type decoupling consisting of multiple slits of equal size is presented. This fence structure acts as bandstop filter which reduces the coupling current between the ports. In [7], a two-port planar inverted F-antenna (PIFA) is discussed for wideband application. In this design, an orthogonal feeding structure is introduced to obtain polarization diversity and reduce mutual coupling between the ports.

---

*Received 6 June 2022, Accepted 20 August 2022, Scheduled 2 September 2022*

\* Corresponding author: Anirban Karmakar (anirban.ece@gmail.com).

<sup>1</sup> Electronics & Communication Engineering Department, Tripura University, India. <sup>2</sup> AEIE Dept., Netaji Subhash Engineering College, Garia, Kolkata, India.

Printed antennas are used in different attractive applications owing to their small size and low cost, but they also have a drawback like high metallic and surface wave losses. These types of problems create a serious issue at higher frequencies which also affect the performance of the antenna. To minimize these drawbacks of a patch antenna, dielectric resonators have been introduced with lots of advantages namely better efficiency, negligible amount of metallic losses, improved gain, etc. So, DRA can be chosen as an appropriate candidate for MIMO antenna system. Some research papers on dielectric resonator (DR)-based MIMO antennas for single-band, multiband, and wideband applications are available in the open literature. In [8], a triple band MIMO DRA is presented. In this design, protruded ground plane is used to improve the isolation between the ports. However, the antenna is very large in size. A dual band hybrid MIMO DRA for wideband application is presented in [9]. In this design, a defected ground structure consisting of dual L-shape slots and a rectangular slot is used to improve the isolation. The antenna occupies a large space and provides narrower impedance bandwidth. A two element MIMO antenna with a ring-DRA is presented in [10] for wideband applications. The presence of the DR and stepped slot provides wide impedance bandwidth and also generates more resonance frequencies. The proposed MIMO antenna also achieves high isolation due to symmetrically oriented antenna elements and generation of opposite currents on the ground plane due to stepped slots. The antenna provides narrower operating bandwidth than the proposed antenna. A dual port rectangular dielectric resonator antenna (RDRA) is presented in [11]. In this design, the mutual coupling problem between the antenna elements is reduced by introducing two symmetrical microstrip feed lines to excite orthogonal modes. However, the size of the antenna is large. A two port MIMO antenna with single rectangular shape DRA for 4G application is presented in [12]. In this design, the DR is placed on the substrate, and two microstrip lines are there to apply the feed to the DR. The two ports create the same mode inside the RDRA in this antenna configuration. The use of two slits in the ground plane has increased the isolation between the ports. However, putting the DR in the substrate complicates the fabrication process. In [13], a multiple-input-multiple-output (MIMO) with rectangular dielectric resonator for LTE applications is presented. Two feeding approaches are used to excite the proposed antenna: a coplanar waveguide (CPW) inductive slot for port 1 and a coaxial probe for port 2. A metallic strip is also added to prolong the electrical length of port 2 so that it can be tuned to 2.6 GHz. In this design, two orthogonal modes are excited by using two different feeding techniques, but the size of the antenna is large. In [14], a MIMO antenna with two rectangular shapes DRs etched on the top of the substrate is presented. In this design, three rectangular shape slots are etched on the ground plane which is placed on the back side of the substrate to reduce the mutual coupling between antenna elements. In addition, the size of the antenna is large with narrow impedance bandwidth. In [15], a dual band MIMO dielectric resonator antenna is presented for WiMAX and WLAN applications. In this design, by using a hybrid feeding mechanism high port isolation is obtained, and two orthogonal modes are excited at each frequency band. However, the size of the antenna is large, and the design is also complex. In [16], a rectangular DR is excited by two ports for designing a MIMO antenna system. Two rectangular strip lines located diagonally opposite the DR's edges stimulate a rectangular DR. To generate the circular polarisation, the ground plane is modified by etching an inverted Z-shaped slot. In [17], a UWB MIMO configuration with a rectangular DR is presented. For UWB applications, a coplanar waveguide (CPW) fed stair-shaped dual rectangular dielectric resonator antenna (RDRA) with different permittivities is developed. In this design, radiators are placed in an orthogonal direction, and to improve isolation between DRs, a diagonal stub is overextended symmetrically in between DR assemblies at a 45-degree angle for controlling the current path. However, this antenna structure requires two pairs of DRs which makes the fabrication expensive. A rack-shaped MIMO dielectric resonator antenna for UWB applications is presented in [18]. In this design, two rectangular radiators with a rack shape DR are used. To improve impedance matching, one stub is introduced in the ground plane. The fabrication process is complex due to rack shape DRs.

In this communication, an angular feed compact UWB MIMO antenna with a band notch is presented. The dimension of the designed antenna is  $19 \times 30 \times 0.8 \text{ mm}^3$ . The proposed antenna utilizes the property of DR to achieve wide impedance bandwidth from 3.1 to 18.5 GHz. In this work, port isolation enhancement is achieved by introducing a modified Hilbert curve and meander line shape parasitic element. The notching at the WLAN band is achieved by introducing a pair of L-shape slots on each rectangular shape radiator.

## 2. ANTENNA DESIGN

The geometrical representation and schematic layout of the proposed two port MIMO antenna and its ground plane are given in Figs. 1(a)–(f). The monopole antenna comprises symmetrical shape rectangular radiators along with rectangular DRs which are excited by an angular feed line. The radiators share common ground plane which is placed on the opposite side of the substrate. For achieving band notch in the WLAN band, a pair of L-shape slots are etched on the radiators. The dimension of the proposed dual port MIMO antenna is  $19 \times 30 \times 0.8 \text{ mm}^3$ . FR4 material characterized by dielectric constant ( $\epsilon_r$ ) of 4.4 and loss tangent of 0.02 is selected as dielectric material for the proposed antenna design. The thickness of the substrate is 0.8 mm. The optimized antenna parameters are given in Table 1.

**Table 1.** Optimized dimension of the MIMO antenna.

Parameter	Dimension (mm)	Parameter	Dimension (mm)	Parameter	Dimension (mm)
$L$	19	$h_2$	9	$L_2$	2.18
$W$	30	$h_3$	7.05	$L_3$	0.2
$L_P$	2.75	$h_4$	4.05	$L_4$	0.6
$W_P$	4.3	$h_5$	1.95	$L_5$	0.75
$L_{DR}$	7.9	$h_6$	1.95	$L_6$	0.2
$W_{DR}$	5	$h_7$	1.95	$p_1$	3.4
$l_{f1}$	2.65	$h_8$	0.9	$p_2$	4.45
$l_{f2}$	2.5	$h_9$	1.95	$p_3$	1.45
$l_{f3}$	4.15	$h_{10}$	0.9	$p_4$	3.5
$W_f$	2	$h_{11}$	1.95	$p_5$	2.3
$W_{f1}$	1	$h_{12}$	0.9	$p_6$	0.6
$L_G$	7	$h_p$	3		
$w_g$	6.9	$H$	5		
$h_1$	12	$L_1$	2.38		

The top view of the designed antenna is shown in Figs. 1(a) and (b). The designed radiator is the combination of two identical shape monopole antennas. Each radiator consists of a rectangular shape metallic patch along with rectangular dielectric resonators. The thickness of each of the dielectric resonator is 5 mm. Angular shape feeding structure is used in this design to provide feed to the radiators. The reason behind using this feeding structure is to minimize the mutual coupling between the antenna elements due to feed excitation. The length of the rectangular patch relates with the first resonance frequency by using the following Equation (1)

$$L_p = \frac{\lambda_g}{4} = \frac{c}{4 \times f_{res}} \quad (1)$$

Here,  $L_p$  represents the length of the patch,  $\lambda_g$  the wave length,  $c$  the speed of light, and  $f_{res}$  the first resonance frequency.  $g$  denotes the distance between two radiating elements. For better performance of a MIMO system, it is necessary to reduce the mutual coupling between radiating elements. According to theory, the DRs have been used to lower the Q-factor so as to widen the bandwidth. Consequently, a relative permittivity around 10 is normally chosen in the proposed design. Alumina ceramic based rectangular DR ( $\epsilon_{r,alumina} = 9.8$ ,  $\tan \delta = 0.002$ ) is placed over monopoles.

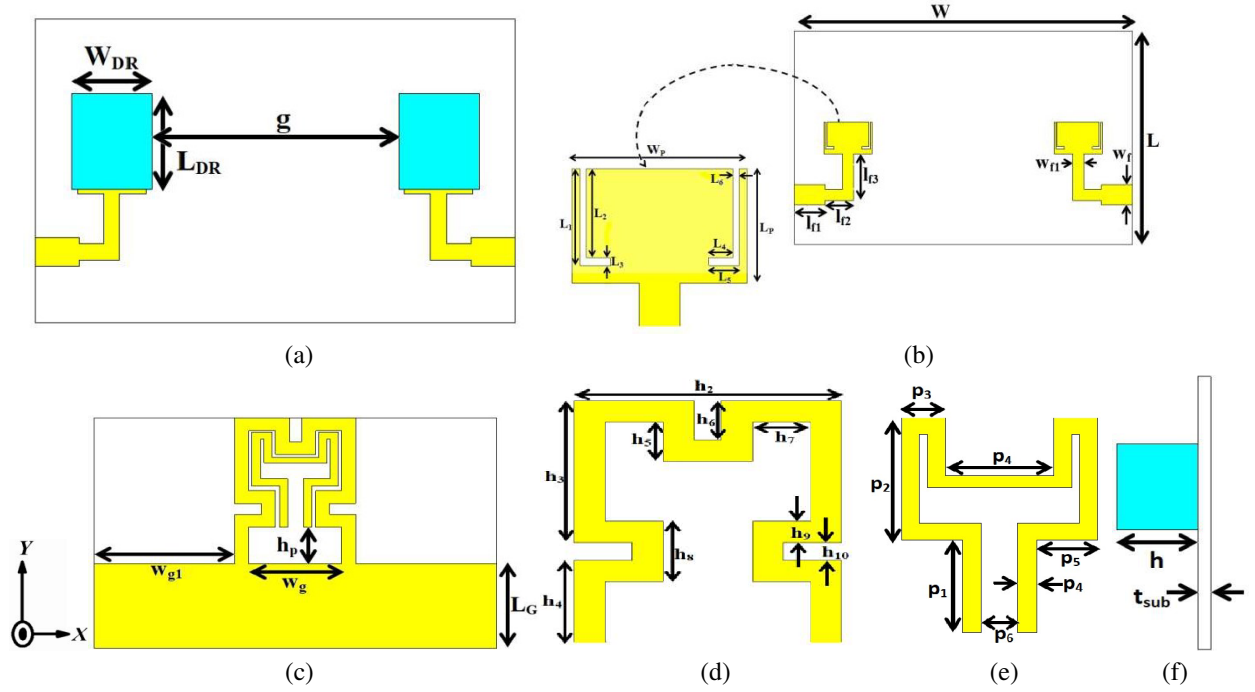


**Figure 1.** Geometrical configuration of proposed antenna. (a) Front view. (b) Dimension of the radiator. (c) Ground plane with isolation structure. (d) Amplified view of modified Hilbert curve (isolation structure). (e) Amplified view of parasitic line. (f) Side view.

The wave numbers of the DR are given by,

$$k_y = \frac{n\pi}{b}, \text{ where } n = 1, 2, 3, \dots \quad (2)$$

$$\text{Similarly, } k_x = \frac{m\pi}{a}, \text{ } m = 1, 2, 3, \dots \quad (3)$$

Transverse Resonance Technique is applied on the air-dielectric boundary, and the wave number thus obtained is a transcendental equation of the form

$$k_z \tan\left(\frac{k_z d}{2}\right) = \sqrt{(\epsilon_r - 1)k_0^2 - k_z^2}, \quad (4)$$

Hence, the wave number for rectangular shape DR is given below,

$$k_x = \frac{\pi}{a}, \quad k_y = \frac{\pi}{b}, \quad k_z \tan\left(\frac{k_z d}{2}\right) = \sqrt{(\epsilon_r - 1)k_0^2 - k_z^2} \quad (5)$$

The wave number satisfies the separation equation,

$$k_x^2 + k_y^2 + k_z^2 = k^2 \quad (6)$$

The resonance frequency of the TE mode can be calculated by using following Equation (7) [12],

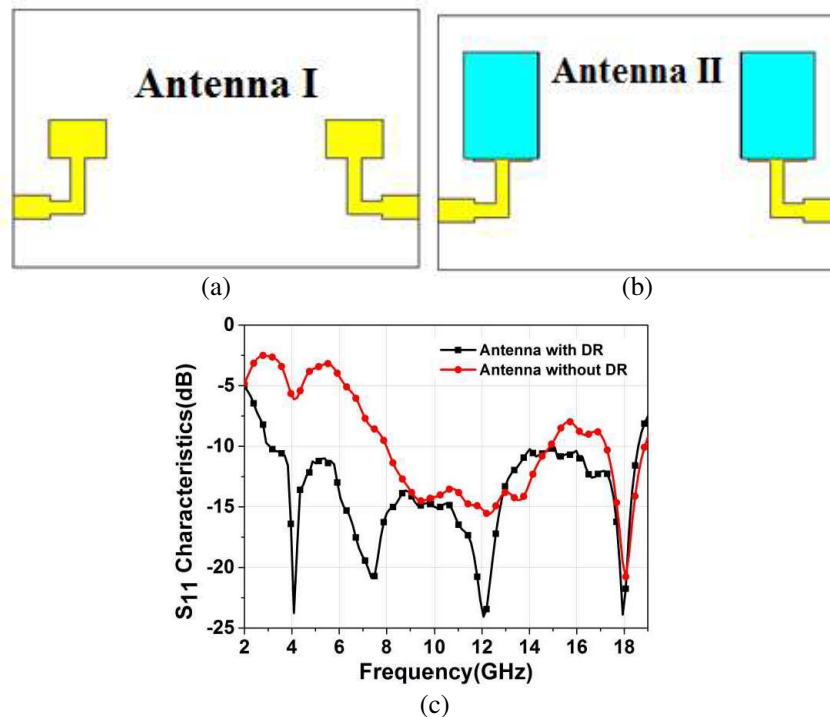
$$f_r = \frac{c}{\sqrt{\epsilon_r}} k = \frac{c}{\sqrt{\epsilon_r}} \sqrt{k_x^2 + k_y^2 + k_z^2} \quad (7)$$

In the above equation,  $c$  is the speed of the light in vacuum;  $f_r$  is the resonance frequency; and  $k_x$ ,  $k_y$ ,  $k_z$  represent the wave numbers of DR in  $x$ -,  $y$ -, and  $z$ -directions, respectively.  $k_0$  represents the wave number in free space, and  $a$ ,  $d$ ,  $b$  are the length, width, and height of the DR, respectively.

The ground plane is etched on the opposite side of the substrate which is shown in Fig. 1(c). In this proposed antenna design, modified Hilbert fractal [19] curve is introduced in the ground plane. To improve the isolation between antenna elements, a meander line parasitic element is placed inside the

Hilbert fractal curve. The meander shape parasitic line has the advantage that it does not occupy extra space but enhances isolation. The amplified view of the Hilbert curve and parasitic element are shown in Figs. 1(d) and (e), respectively. The side view of the proposed antenna is shown in Fig. 1(f).

In order to understand the reason behind the creation of each resonant peak, the proposed antenna is classified as Antenna I and Antenna II as shown in Figs. 2(a)–(b). Antenna I consists of a conventional rectangular shape metallic patch element with an angular feeding structure. In Antenna II, a rectangular shape DR element is introduced over the patch element.



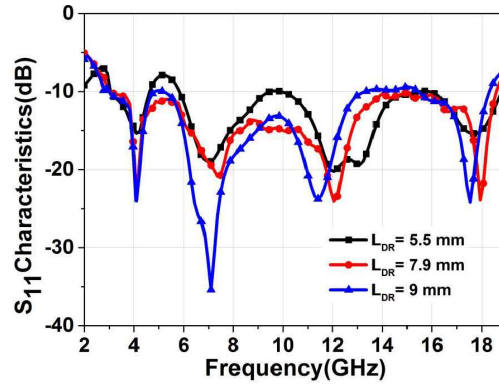
**Figure 2.** Configuration and reflection coefficient of Antenna-I and II. (a) Configuration of Antenna I. (b) Configuration of Antenna II. (c) Comparison of simulated  $S_{11}$  characteristics.

Figure 2(c) shows the effect of DR on  $S_{11}$  parameter. It is noticed from the plot that due to the presence of the DR element different resonance peaks are generated. The presence of the DR also enhances the bandwidth of the proposed antenna and shifts the lower band toward lower frequencies. After introducing the DR, the antenna provides a bandwidth from 3.1 to 18.5 GHz.

Figure 3 shows the effect of the length of DR ( $L_{DR}$ ) on the reflection coefficient of the antenna. It can be seen from the plot that when we choose 7.9 mm as length of the DR, the proposed antenna provides wider operating bandwidth than the other dimensions. So, we choose 7.9 mm as the length of the DR element for the proposed design.

### 2.1. Isolation Structure

The ground plane always plays a crucial role for improving the performance of a MIMO antenna. Here it not only improves the impedance matching of the antenna elements but also enhances the isolation between them. Hilbert shape fractal curve is a type of continuous fractal space filling curve, which was first introduced by German mathematician David Hilbert in 1891 [19, 20]. Hilbert curve geometry is introduced in antenna design to miniaturize the size of isolation structure. The presence of the fractal structure also enhances the effective electrical length of the isolation structure without employing much area [19]. For this characteristic, the overall antenna size becomes very compact. Fig. 4 shows the different iterations of Hilbert fractal curve. It is observed that the total length of the Hilbert curve



**Figure 3.** Effect of the length of DR on  $S_{11}$  characteristics.

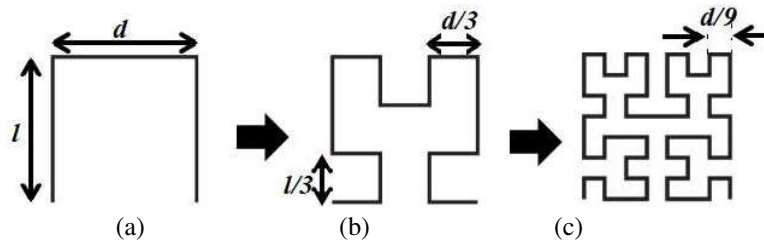


**Figure 4.** Hilbert-curves with different iteration. (a) 0th iteration, (b) 1st iteration, and (c) 2nd iteration.

increases with every iteration, but it keeps overall area constant.

The sum  $S$  of all the line segments of Hilbert curve is given by the following equations [20],

$$S = (2^{2n} - 1)d = (2^n + 1)l \quad (8)$$

$$\text{where } d = \frac{l}{(2^n - 1)} \quad (9)$$

In Equation (8),  $l$  represents the side dimension of the Hilbert-curve,  $d$  the length of each line segment, and  $n$  the order of iteration. In this article, the Hilbert-curve with the second order is used. Figs. 5(a)–(c) show the evolution of the isolation structure. The effect of the isolation structure on  $S_{21}$  parameter of the antenna elements is depicted in Fig. 5(e). From the  $S_{21}$  characteristics we can see that the proposed MIMO antenna provides poor isolation when a conventional rectangular shape ground plane is used (Case I) as shown in Fig. 5(a). After that in order to enhance the isolation as well as to lower the mutual coupling between the antenna elements, a modified Hilbert curve is introduced as an isolation structure as shown in Figs. 5(b)–(d). In Fig. 5(b), the 0th iteration of the Hilbert curve is given. After that, the 1st iteration of the Hilbert curve is introduced as depicted in Fig. 5(c). In CASE IV, a meander shape parasitic line is introduced inside the Hilbert fractal curve for the further reduction of mutual coupling between the antenna elements as shown in Fig. 5(d).

The presence of the modified Hilbert shape curve improves the isolation between the antenna elements as shown in Fig. 5(e). The  $S_{21}$  characteristic improves with every iteration of fractal curve. The parasitic element reduces the effect of mutual coupling between the antenna elements and provides isolation from 3.1 to 18.5 GHz.

To further understand the effect of decoupling structure, surface current distribution is shown in Fig. 6. Fig. 6(a) shows the surface current distribution for conventional rectangular shape ground plane when port 1 is activated and port 2 terminated to  $50\Omega$  load. It is revealed from the surface current distribution that maximum amount of the current concentrates towards port 1 as compared to that of port 2. In Fig. 6(b), a modified Hilbert curve is introduced to reduce the effect of mutual coupling. In this design, Hilbert fractal curve up to the 1st iteration is initiated to enhance the isolation between the ports. It is also noticed from Fig. 6(b) that the Hilbert fractal curve concentrates most of the current.

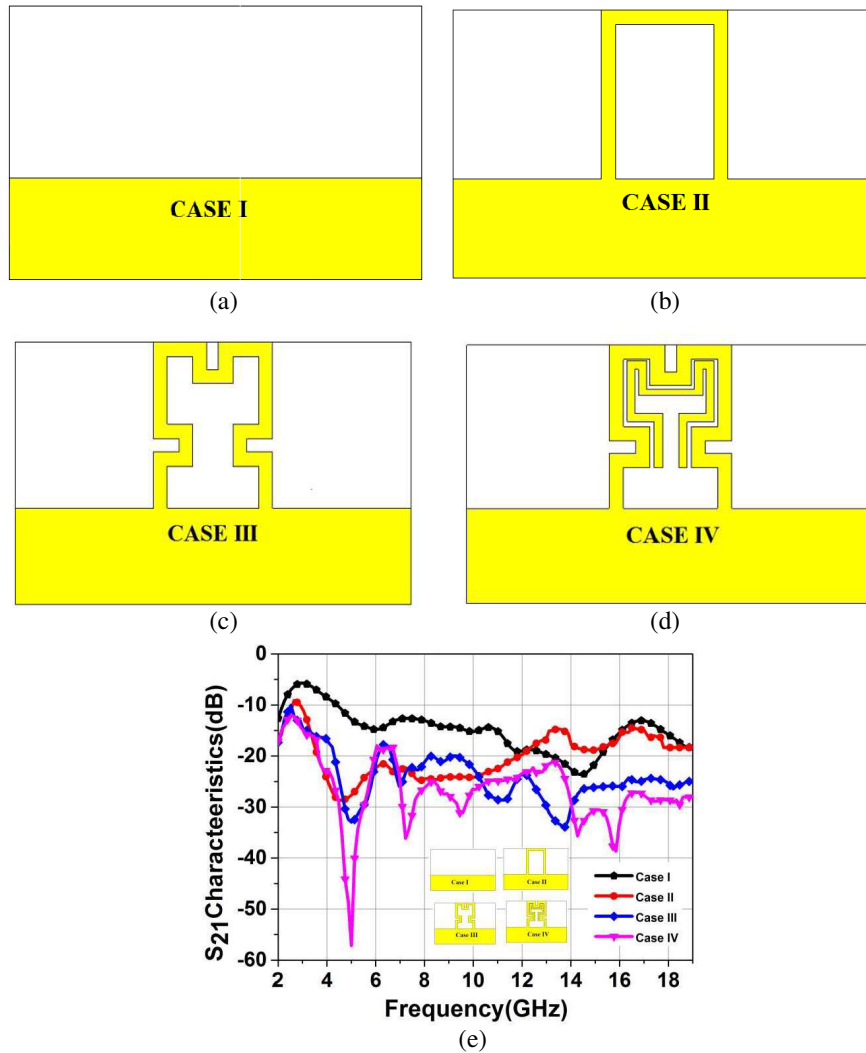


**Figure 5.** Evolution of isolation structure. (a) Rectangular ground plane. (b) Rectangular ground plane with 0th iteration Hilbert fractal curve. (c) Rectangular ground plane with 1st iteration Hilbert fractal curve. (d) Rectangular ground plane with 1st iteration Hilbert fractal curve and meander shape parasitic line. (e) Comparison of  $S_{21}$  among Case I, Case II, Case III and Case IV.

A meander line parasitic element is placed inside the modified Hilbert shape isolation structure to further reduce the mutual coupling between the ports.

It can be revealed from Fig. 6(c) that the presence of the parasitic element reduces the mutual coupling between ports 1 and 2. It can also be observed that maximum amount of current concentrates on the parasitic element, which shortens the flow of power between the two ports. Consequently, the mutual coupling between the two ports is reduced.

Figures 7(a)–(d) depict the  $E$ -field distribution inside the two DRs at 4.2 GHz when port 1 and port 2 are excited respectively. From Fig. 7(a) it is noticed that when port 1 is excited and port 2 terminated to  $50\ \Omega$ , the  $TE_{11\delta}^z$  mode is excited at 4.2 GHz in DR1 (which is associated with port 1). Fig. 7(b) shows the side view when port 1 is excited and port 2 terminated; the  $TE_{11\delta}^z$  mode is excited at 4.2 GHz in DR1. Figs. 7(c), (d) show the front and side views of  $E$ -field distribution when port 2 is excited and port 1 terminated to 50 ohm load. In both the cases,  $TE_{1\delta 1}^y$  modes are generated. The subscripts present in  $TE_{11\delta}$  mode denote the half-wave variation along  $X$ -axis direction, half-wave variation along  $Y$ -axis direction, and  $\delta$  depicts the field variation in between modes 0 and 1. In this design, DR also enhances the bandwidth of the proposed antenna.

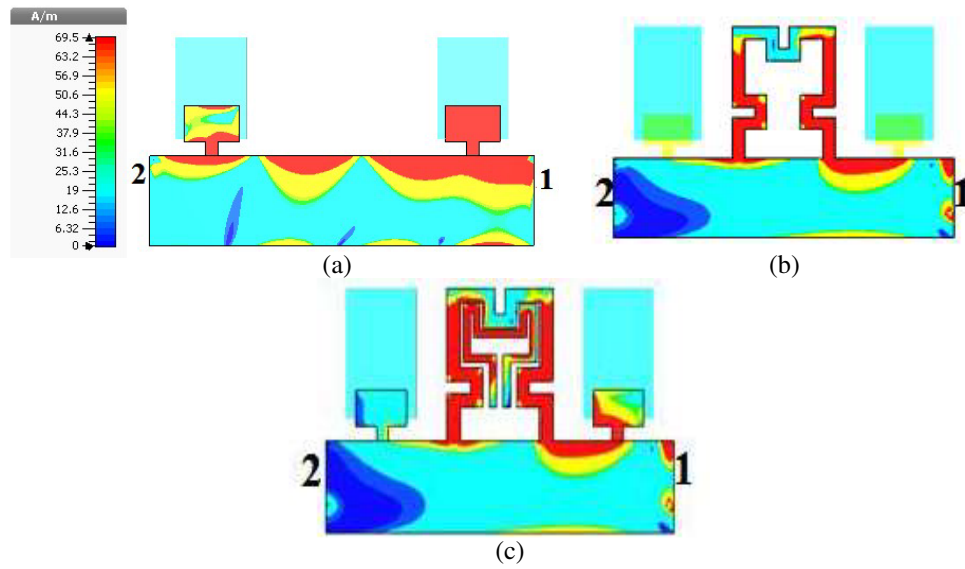


**Figure 6.** Current distribution at different geometry of the isolation structure at 5 GHz. (a) Rectangular ground plane. (b) Modified Hilbert curve. (c) Modified Hilbert curve with meander line parasitic element (When Port 1 is activated and Port 2 is terminated).

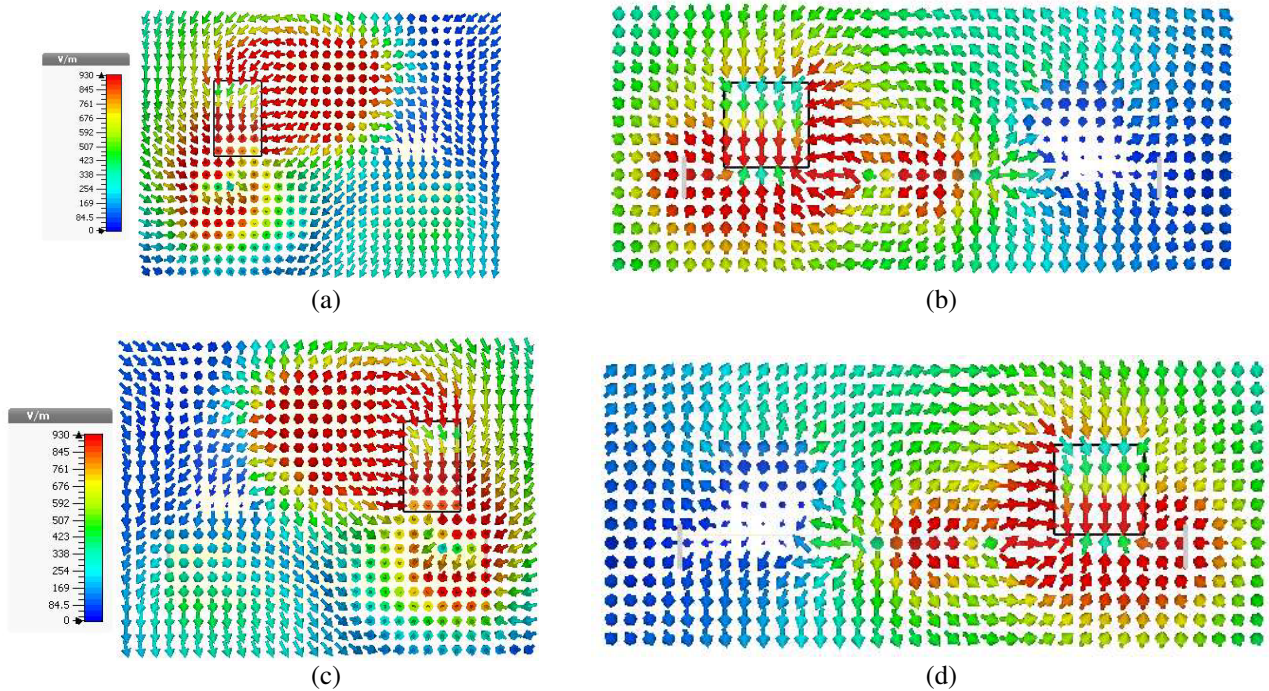


**Figure 7.** Electric field distribution in dielectric resonator at 4.2 GHz. (a) Front view when Port 1 excited. (b) Side view when Port 1 is excited. (c) Front view when port 2 excited. (d) Side view when Port 2 excited.

## 2.2. Role of Slot on the Radiator Structure

The band notch characteristics in the proposed antenna can be achieved by etching two pairs of identical L-shape slots on each radiator. The L-shape slots provide a band notch at WLAN band ranging from

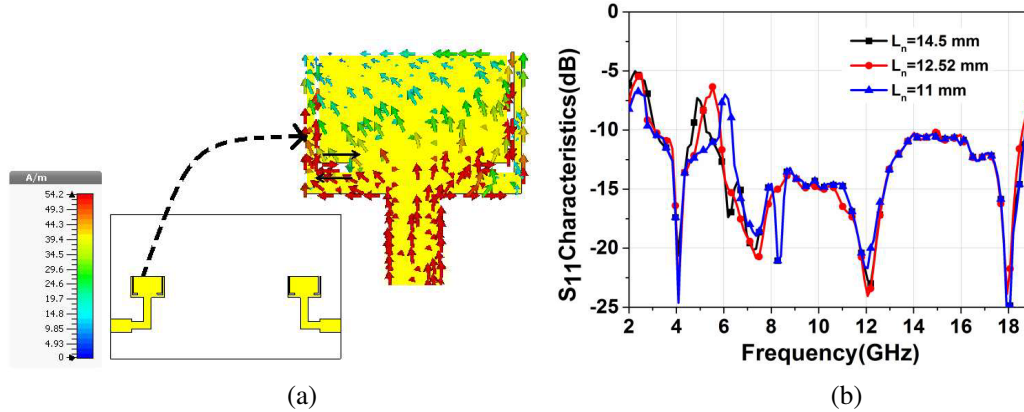


**Figure 8.** Notching structure. (a) Current distribution on the strip at 5.5 GHz. (b)  $S$  parameter for various values of  $L_n$ .

5.09–5.8 GHz with center frequency at 5.5 GHz. It can be noticed from Fig. 8(a) that surface current mainly concentrates on the slot at 5.5 GHz. The vector directions of the surface current along the sides of L-shape slots are in the opposite direction. Therefore, the radiation generated from one side current will be cancelled by the other side current, so no radiation occurs, and the corresponding return loss is poor in that particular frequency. Fig. 8(a) depicts the current distribution of the slot, and it is observed that the proposed MIMO antenna can effectively offer a band-notching at WLAN band.

Figure 8(b) shows the effect of slot length on the  $S$ -parameter. It can be observed from the parametric study of  $L_n$  that if we increase slot length beyond 12.52 mm, the centre of the notch frequency band shifts to the lower frequency end. On the other hand, if we lower the slot length below 12.52 mm, the centre of the notch band shifts towards higher frequency end.

So, we have chosen 12.52 mm as optimized slot length which achieves band notch at the centre frequency of WLAN band. These L-shape slots present in the radiator work as a quarter-guided-wavelength resonator. The length of each slot can be provisionally approximated by Equation (10) [21]:

$$L_n = 4(L_1 + L_2 + L_3 + L_4 + L_5 + L_6) \tag{10}$$

The length  $L_n$  for the centre frequency of band-rejection achieved at WLAN band is 12.52 mm which can be calculated as [21]

$$f_n = \frac{c}{2L_n\sqrt{\epsilon_{reff}}} \tag{11}$$

In the above Equation (11),  $c$  is used to represent the speed of light, and  $\epsilon_{reff}$  denotes the effective dielectric constant of the substrate; it will almost equal to the half of the dielectric constant of the substrate material.

### 3. RESULTS AND ANALYSIS

Commercial electromagnetic simulation software CST is used to simulate this proposed dual port MIMO antenna structure. The proposed antenna is fabricated, and its bandwidth performance is measured by using Agilent E5071C vector network analyzer (VNA). Fig. 9 shows the front and back views of the fabricated prototype.

The simulated and measured scattering parameters of the designed MIMO antenna structure are given in Fig. 10. The  $S$ -parameters for both ports remain same due to symmetric structure of the MIMO antenna.

It can be revealed from the above plot that the designed antenna provides bandwidth ( $< -10$  dB) from 3.1 to 18.5 GHz. In this operating bandwidth range band notching is achieved at WLAN band (5.09–5.8 GHz). Fig. 10 also shows the simulated and measured  $S_{21}$  characteristics which shows that proposed antenna provides isolation better than  $-15$  dB from 3.1 to 4 GHz and better than  $-20$  dB for rest of the frequency range.



**Figure 9.** Fabricated prototype of the designed antenna. (a) Top view. (b) Back view.

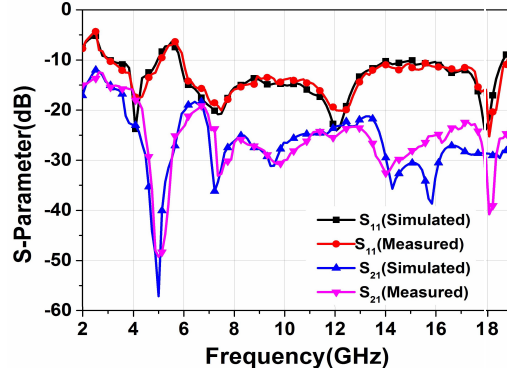


**Figure 10.** Simulated and measured  $S$ -parameter of the designed antenna.

The 2D  $E$ - and  $H$ -field co-pole and cross-pole patterns (simulated and measured) of the designed antenna at 4.2 GHz, 7.3 GHz, and 10 GHz are shown in Figs. 11(a), (b), & (c). It is obtained when port 1 is excited and port 2 terminated by  $50 \Omega$  load.

Normally, cross polarization is always orthogonal to the co-polarization. For example, if the fields generated by the designed antenna are horizontally polarized, then the cross polarization in this case will be vertically polarized, which means directed in the vertical direction. It is observed from the co-pole and cross-pole plots that the designed antenna provides almost an omnidirectional radiation pattern over the entire operating frequency range, but at higher frequencies, the radiation patterns deteriorate due to breaking of radiation lobes. The measured gain of the designed MIMO antenna is shown in Fig. 12. The gain increases with increasing operating frequencies and drops at notch frequency band. Fig. 12 also represents the radiation efficiency of the proposed antenna. It is observed that the proposed radiator obtains very good radiation efficiencies ( $> 80\%$ ) in the operating band.

#### 4. MIMO PERFORMANCE

The working of the designed MIMO antenna is examined with respect to some parameters namely Envelope Correlation Coefficient (ECC) and Diversity Gain (DG). The use of ECC [22] is to specify the quantity of correlation present among the elements in antenna. The calculated ECC value can be obtained from Equation (12) which is given below. For an uncorrelated diversity antenna, the ideal value of ECC is zero, but the practical acceptable value is less than 0.5. The ECC value of the designed antenna can be calculated from radiation pattern by Equation (12) [23].

$$ECC = \frac{\left| \iint_{4\pi} [\vec{F}_1(\theta, \varphi) * \vec{F}_2(\theta, \varphi)] d\Omega \right|^2}{\iint_{4\pi} |\vec{F}_1(\theta, \varphi)|^2 d\Omega \iint_{4\pi} |\vec{F}_2(\theta, \varphi)|^2 d\Omega} \quad (12)$$

In Equation (12),  $F_i(\theta, \phi)$  represents the three-dimensional field radiation pattern of the proposed antenna when the  $i$ th port is excited, and  $\Omega$  represents the solid angle. The asterisk in the equation is the Hermitian product operator. The parameter diversity is usually realised when the transmitter

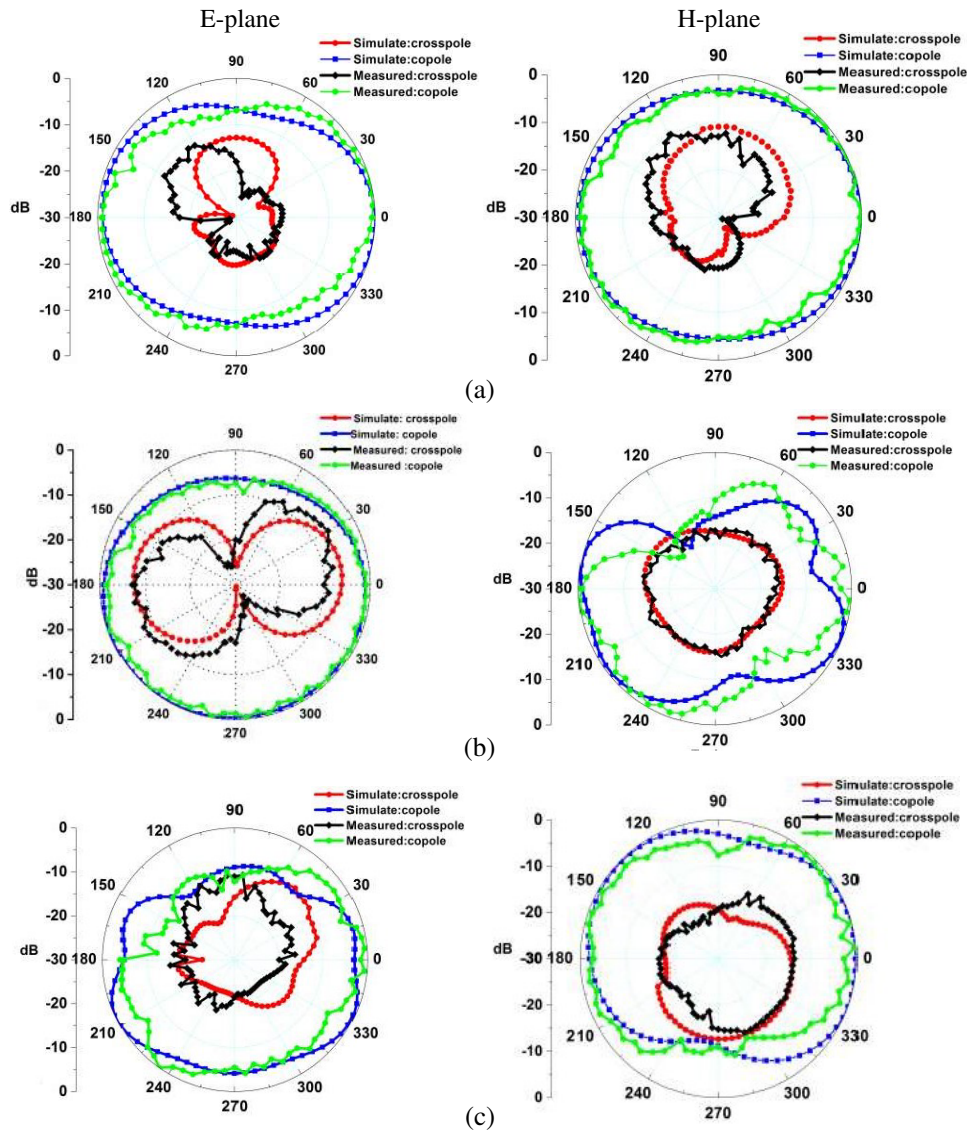


**Figure 11.** Simulated and measured *E* plane and *H* plane co-pole and cross-pole radiation patterns at (a) 4.2 GHz, (b) 7.3 GHz, (c) 10 GHz.

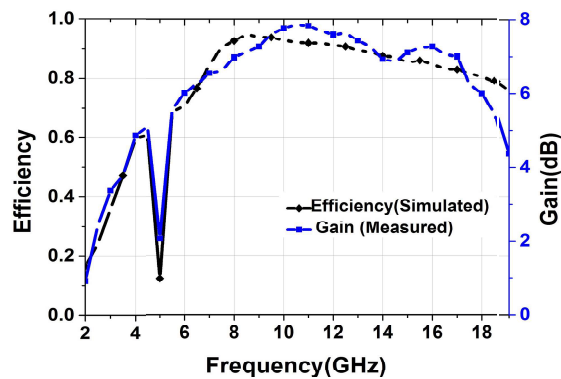


**Figure 12.** Efficiency and gain plot of the designed antenna.

accepts multiple numbers of the transmitted stream through different channel paths (since we have multiple antennas). If the received signals are uncorrelated in nature, then combined signals at the receiver end will provide higher signal-to-noise-ratio levels, and thus achieve better signal reception.

Diversity gain (DG) calculates the effectiveness of diversity on the communication system performance. The term “diversity” depicts the dissimilarity present in the time-averaged Signal to Noise Ratio of the combined signals within the diversity antenna system and that of a single antenna system in one diversity channel. The value of DG for the designed antenna can be calculated from ECC parameter by using the following equation [23]

$$DG = 10\sqrt{1 - ECC^2} \quad (13)$$

The value of diversity gain obtained from Equation (13) is higher than 9.95 dB. Fig. 13 represents simulated and measured curves for ECC and diversity gain. It is exhibited from the plot that simulated and measured values of ECC lie below 0.01. Fig. 13 also shows the simulated and measured curves of DG, which offers a diversity gain better than 9.95 dB over the entire frequency range.

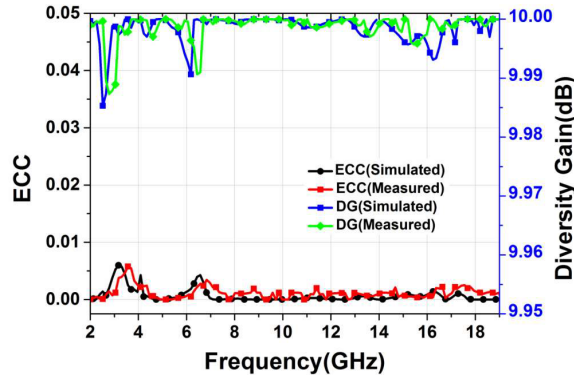


**Figure 13.** Simulated ECC and diversity gain of designed antenna.

To highlight the originality of the proposed work, Table 2 shows a comparison of the performances of the previously related works and the proposed one. The proposed antenna has a more compact size

**Table 2.** Comparison of the proposed MIMO antenna with other relatable published work.

References	Size (mm <sup>2</sup> )	Bandwidth (GHz)	Isolation (dB)	Gain (dB)	ECC
[8]	48 × 70	1.86–6.75	Below –18	5	< 0.01
[9]	59 × 55	3–7	Below –18	5.5	< 0.21
[10]	31 × 50	3.3–8.2	Below –20	5	Not available
[11]	90 × 90	1.7–1.9	Below –18	Not available	< 0.01
[12]	80 × 80	2.56–2.64	Below –20	Not available	< 0.1
[13]	70 × 70	2.44–3.38	Below –20	Not available	
[14]	80 × 120	1.6–2.11	Below –17	Not available	< 0.0125
[15]	60 × 60	3.23–5.86	Below –40	6.1	< 0.009
[16]	30 × 36	5.4–7.4	Below –15	3.5	< 0.02
[17]	48 × 48	1.6–12.2	Below –25	4.72	< 0.005
[18]	39.6 × 29	3.54–10.87	Below –21	5.5	< 0.007
<b>Proposed work</b>	<b>19 × 30</b>	<b>3.1–18</b>	<b>Below –20</b>	<b>7.9</b>	<b>&lt; 0.01</b>

and wider operating bandwidth than the other MIMO antennas reported in [7–18]. Also, the proposed antenna has provided better isolation than [8, 9, 11, 14, 16]. Many researchers presented MIMO antennas with fractal isolation structures [24, 25]. In [24], a complex design consists of a parasitic element and Hilbert fractal defects which are used in the ground to improve the isolation. In [25], again a Hilbert slot is used in the ground plane to achieve better isolation. Both the designs contain larger area as than the proposed antenna design. The designed antenna has a compact size with low mutual coupling, hence provides a viable solution for many portable wireless applications.

## 5. CONCLUSION

In this article, A dual port compact angular feed MIMO antenna with UWB application is presented. The characteristics have been achieved by exciting rectangular shape Dielectric resonator along with the radiator. The isolation is achieved by introducing A modified Hilbert shape fractal curve along with a meander shape parasitic line. Consequently, the proposed radiator attains isolation more than  $-20$  dB in the whole working frequency band. The diversity performance of the antenna is also studied, and the simulated results indicate that the designed MIMO antenna is an appropriate candidate for different areas of portable wireless communications.

## REFERENCES

1. “Revision of part 15 of the commissions rules regarding ultra-wideband transmission systems first report and order FCC 02.V48,” *Federal Communications Commission*, Tech. Rep., Washington, DC, 2002.
2. Zhengand, L. and N. C. Tse, “Diversity and multiplexing: A fundamental tradeoff in multiple-antenna channels,” *IEEE Transaction of Information Theory*, Vol. 49, No. 5, 1073–1096, 2003.
3. Zhou, Q. and H. Dai, “Joint antenna selection and link adaptation for MIMO systems,” *IEEE Transactions on Vehicular Technology*, Vol. 55, No. 1, 243–255, 2006.
4. Luo, C., J. Hong, and L. Zhong, “Isolation enhancement of a very compact UWB-MIMO slot antenna with two defected ground structures,” *IEEE Antennas and Wireless Propagation Letters*, Vol. 14, 1766–1769, 2015.
5. Li, J., Q. Chu, and T. Huang, “A compact wideband MIMO antenna with two novel bent slits,” *IEEE Transactions on Antennas and Propagation*, Vol. 60, No. 2, 482–489, 2012.
6. Wang, L., et al., “Compact UWB MIMO antenna with high isolation using fence-type decoupling structure,” *IEEE Antennas and Wireless Propagation Letters*, Vol. 18, No. 8, 1641–1645, 2019.
7. Chattha, H. T., M. Nasir, Q. H. Abbasi, Y. Huang, and S. S. AlJa’afreh, “Compact low-profile dual-port single wideband planar inverted-F MIMO antenna,” *IEEE Antennas and Wireless Propagation Letters*, Vol. 12, 1673–1675, 2013.
8. Das, G., A. Sharma, and R. K. Gangwar, “Triple-band hybrid antenna with integral isolation mechanism for MIMO applications,” *Microwave Opt. Technology Letter.*, Vol. 60, No. 6, 1482–1491, 2018.
9. Kumari, T., G. Das, and A. Sharma, “Design approach for dual element hybrid MIMO antenna arrangement for wideband applications,” *International Journal of RF and Microwave Computer-Aided Engineering*, Vol. 29, No. 1, 1–10, 2019.
10. Das, G., A. Sharma, and R. K. Gangwar, “Wideband self-complementary hybrid ring dielectric resonator antenna for MIMO applications,” *IET Microwaves, Antennas & Propagation*, Vol. 12, No. 1, 108–114, 2018.
11. Nasir, J., M. H. Jamaluddin, M. Khalily, M. R. Kamarudin, and I. Ullah, “A reduced size dual port MIMO DRA with high isolation for 4G applications,” *International Journal of RF and Microwave Computer-Aided Engineering*, Vol. 25, No. 6, 495–501, 2015.
12. Nasir, J., M. H. Jamaluddin, M. Khalily, M. R. Kamarudin, and I. Ullah, “Design of an MIMO dielectric resonator antenna for 4G applications,” *Wireless Personal Communications*, Vol. 88, 525–536, 2016.

13. Roslan, S. F., M. R. Kamarudin, M. Khalily, and M. H. Jamaluddin, "An MIMO rectangular dielectric resonator antenna for 4G applications," *IEEE Antennas and Wireless Propagation Letters*, Vol. 13, 321–324, 2014.
14. Selvaraju, R., M. R. Kamarudin, M. Khalily, M. H. Jamaluddin, and J. Nasir, "Dual-port MIMO rectangular dielectric resonator antenna for 4G-LTE application," *Applied Mechanics and Materials*, Vol. 781, 24–27, 2015.
15. Khan, A. A., R. Khan, S. Aqeel, J. Nasir, and J. Saleem, "Design of a dual-band MIMO dielectric resonator antenna with high port isolation for WiMAX and WLAN applications," *International Journal of RF and Microwave Computer-Aided Engineering*, Vol. 17, No. 2, 1–11, 2017.
16. Kumar, V., "Rectangular DR-based dual-band CP-MIMO antenna with inverted Z-shaped slot," *International Journal of Electronics*, Vol. 107, No. 10, 1559–1573, 2020.
17. Sani, M. M., R. Chowdhury, and R. K. Chaudhary, "An ultra-wideband rectangular dielectric resonator antenna with MIMO configuration," *IEEE Access*, Vol. 8, 139658–139669, 2020.
18. Yadav, S. K., A. Kaur, and R. Khanna, "Compact rack shaped MIMO dielectric resonator antenna with improved axial ratio for UWB applications," *Wireless Personal Communication*, Vol. 117, 591–606, 2021.
19. Karmakar, A., "Fractal antennas and arrays: A review and recent developments," *International Journal of Microwave and Wireless Technologies*, Vol. 13, No. 2, 1–25, 2020.
20. Karmakar, A., S. Verma, M. Pal, and R. Ghatak, "An ultra wideband monopole antenna with multiple fractal slots with dual band rejection characteristics," *Progress In Electromagnetics Research C*, Vol. 31, 185–197, 2012.
21. Gautam, A. K., A. Saini, N. Agrawal, and N. Z. Rizvi, "Design of a compact protrudent-shaped ultra-wideband multiple-input multiple-output/diversity antenna with band-rejection capability," *International Journal of RF and Microwave Computer-Aided Engineering*, Vol. 29, No. 9, 1–11, 2019.
22. Blanch, S., J. Romeu, and I. Corbella, "Exact representation of antenna system diversity performance from input parameter description," *Electronics Letters*, Vol. 39, No. 9, 705–707, 2003.
23. Sharawi, M. S., "Printed multi-band MIMO antenna systems and their performance metrics," *IEEE Antennas and Propagation Magazine*, Vol. 55, No. 5, 218–232, 2013.
24. Banerjee, J., A. Gorai, and R. Ghatak, "Design and analysis of a compact UWB MIMO antenna incorporating fractal inspired isolation improvement and band rejection structures," *International Journal of Electronics and Communications (AEÜ)*, Vol. 122, 1–9, 2020.
25. Gorai, A., A. Dasgupta, and R. Ghatak, "A compact quasi-self-complementary Dual Band Notched UWB MIMO Antenna with enhanced isolation using Hilbert fractal slot," *International Journal of Electronics and Communications*, Vol. 94, 36–41, 2018.